Characterizing the Distribution of Nonylphenol Ethoxylate Surfactants in Water-Based Pressure-Sensitive Adhesive Films using Atomic-Force and Confocal Raman Microscopy

Guizhen H. Xu,[†] Jinping Dong,[‡] Jiguang Zhang,[†] Steven J. Severtson,*[,†] Carl J. Houtman,[§] and Larry E. Gwin[||]

Department of Bioproducts and Biosystems Engineering, University of Minnesota, 2004 Folwell Ave., St. Paul, Minnesota 55108, Characterization Facility, University of Minnesota, 12 Shepherd Laboratories, 100 Union St. S.E., Minneapolis, Minnesota 55455, Forest Products Laboratory, USDA, One Gifford Pinchot Drive, Madison Wisconsin 53726, and Franklin International, 2020 Bruck Street, Columbus, Ohio 43207

Received: June 2, 2008; Revised Manuscript Received: July 22, 2008

Surfactant distributions in model pressure-sensitive adhesive (PSA) films were investigated using atomic force microscopy (AFM) and confocal Raman microscopy (CRM). The PSAs are water-based acrylics synthesized with *n*-butyl acrylate, vinyl acetate, and methacrylic acid and two commercially available surfactants, disodium (nonylphenoxypolyethoxy)ethyl sulfosuccinate (anionic) and nonylphenoxypoly(ethyleneoxy) ethanol (nonionic). The ratio of these surfactants was varied, while the total surfactant content was held constant. AFM images demonstrate the tendency of anionic surfactant to accumulate at the film surfaces and retard latex particle coalescence. CRM, which was introduced here as a means of providing quantitative depth profiling of surfactant concentration in latex adhesive films, confirms that the anionic surfactant tends to migrate to the film interfaces. This is consistent with its greater water solubility, which causes it to be transported by convective flow during the film coalescence process. The behavior of the nonionic surfactant is consistent with its greater compatibility with the polymer, showing little enrichment at film interfaces and little lateral variability in concentration measurements made via CRM. Surfactant distributions near film interfaces determined via CRM are well fit by an exponential decay model, in which concentrations drop from their highs at interfaces to plateau values in the film bulk. It was observed that decay constants are larger at the film−air interface compared with those obtained at the film−substrate side indicating differences in the mechanism involved. In general, it is shown here that CRM acts as a powerful compliment to AFM in characterizing the distribution of surfactant species in PSA film formation.

Introduction

Pressure-sensitive adhesives (PSAs) are those capable of aggressively bonding to most material surfaces simply through the application of light pressure. Water-based PSA films are cast from aqueous colloidal dispersions. Other than the adhesive polymer, the most prevalent chemical in PSA films are emulsifiers, usually composing less than 10 wt % of adhesive films. While mixtures of anionic and nonionic surfactants are used in commercial products, anionic surfactants are often a dominant component. The surfactant is added to allow for the generation of high-solids lattices ensuring stability of colloidal particles of PSA during the polymerization process. However, they are also believed to cause poor adhesive performance due to their heterogeneous distribution in PSA film.[1−5] Depending on the compatibility between surfactant and latex particles, surfactant may partially dissolve into the adhesive polymer, remain at the interfaces between particles and/or phase-separate from the polymeric solution and migrate to film interfaces.[6]

Due to its significance in determining adhesive product performance, the distribution of surfactants in films cast from acrylic latexes has been a matter of interest for many years. It is believed that the main factors influencing the out-of-plane distribution of surfactants includes the chemical nature of the latex system, aging time, film formation environments (temperature and relative humidity) and the structures of the surfactants.[7] For example, Guigner et al. reported very different concentration profiles for a series of surfactants that included sodium dodecyl sulfate, hexadecylpyridinium chloride and hexadecyltrimethylammonium bromide in poly(2-ethylhexyl methacrylate) latex films.[8] Several researchers have reported higher surfactant concentrations at the film interfaces and propose that the enrichment hinders or delays particle coalescence in these regions resulting in weaker films.[9−11] The more pronounced enrichment occurs at the film−air side and results from the aided transportation of free (nonsorbed) surfactant due to the convective movement of water during drying.[12,13] Kientz and Holl[6] suggested that the distribution of surfactant depends on factors such as the initial surfactant distribution at the interfaces, surfactant desorption during drying and the mobility of surfactant in the drying film. Belaroui[14,15] and Mallégol et al.[16−18] argued that the distribution of water and extent of coalescence during drying also play an important role in determining enrichment/depletion of surfactant at film interfaces.

Given the likely importance of surfactant distributions to the performance of a water-based PSA, a number of techniques have been applied to characterize concentration profiles. Fourier transform infrared spectroscopy (FTIR),[6] attenuated total reflec-

* Author to whom correspondence should be addressed. E-mail: sever018@umn.edu. Telephone: (612) 625-5265. Fax: (612) 625-6286.
[†] Department of Bioproducts and Biosystems Engineering, University of Minnesota.
[‡] Characterization Facility, University of Minnesota.
[§] Forest Products Laboratory, USDA.
[||] Franklin International.

10.1021/jp804876x CCC: $40.75
Published on Web 09/03/2008

TABLE 1: Chemical and Physical Properties of Surfactants

properties	anionic surfactant	nonionic surfactant
molecular formula	$C_{15}H_{23}(OCH_2CH_2)_nC_4H_3O_7Na_2S$, $n \approx 11$	$C_{15}H_{23}(OCH_2CH_2)_nOH$, $n \approx 9$
molar mass (g/mol)	$M_n = 905.26$; $M_w = 935.84$	$M_n = 597.54$, $M_w = 608.32$
critical micelle concentration[a] (% by weight)	1.5×10^{-2}	2.1×10^{-4}
hydrophilic−lipophilic balance[a] (HLB)	15	10
log K_{ow}	2.55[b]	3.38

[a] Values reported by the suppliers. [b] Calculated for the free acid form of the molecule.

TABLE 2: Properties of Model PSAs

measurement	PSA 1	PSA 2	PSA 3
anionic:nonionic wt %	100:0	50:50	10:90
latex viscosity (cps)	88	90	750
mean particle size (nm)	450	690	1250
pH	4.39	4.28	4.32
molar mass (g/mol)	$M_n = 25000$, $M_w = 160000$, PDI = 6.4	$M_n = 29841$, $M_w = 260180$, PDI = 8.7	$M_n = 27500$, $M_w = 209000$, PDI = 7.6
glass transition temperature (°C)	−19.8	−34	−24
peel adhesion (lbs)	2.0	2.0	2.1
loop tack (lbs)	2.6	2.3	2.0
178° shear adhesion (min)	300	200	960
contact angle with water (deg)	106	110	112

tion (ATR) FTIR,[6−8,15,19−23] infrared microscopy,[8] X-ray photoelectron spectroscopy,[12] nuclear magnetic resonance,[8,16] and Rutherford backscattering spectroscopy (RBS)[17,24] have been used to collect out-of-plane distribution data of surfactant. However, these techniques either cannot provide layer by layer depth profiling information or only allow for analysis within a few microns of the surface. In fact, most studies published previously examining surfactant-polymer compatibility and mobility of anionic and nonionic surfactants in latex films are based on the results from ATR-FTIR spectra obtained on film−air and film−substrate interfaces.

Confocal Raman microscopy (CRM) is a relatively new technique that has been employed to obtain surfactant distribution information in recent years. It has been shown to be an effective method for the depth profiling of thin films, coatings, membranes and composites.[25,26] This technique allows one to record a Raman spectrum for a small volume of film without any modification of samples by combining a high resolution confocal microscope with a sensitive Raman spectroscopy system. By applying confocal optics, the sampling volume can be moved along a direction perpendicular to the film surface over several tens of micrometers by tuning the plane of focus of the microscope in a stepwise fashion. Differences in chemical composition of a film can be viewed in Raman spectra at various depths. In this paper, CRM is applied to a series of emulsion-type adhesives, based on a commercial, label-grade, water-based acrylic PSA. The adhesives use both anionic and nonionic nonylphenol ethoxylate emulsifiers. By switching the dominant surfactant from anionic to nonionic, information is obtained on the tendency of these different species to migrate. Atomic force microscopy (AFM) was used for imaging both the film−air and film−substrate interfaces to further characterize the migration process and show the impact of migration on the coalescence of latex particles. This combination of quantitative and qualitative high resolution techniques is shown to be a powerful method for characterizing the movement of surfactants in water-based PSA films and their impact on structure.

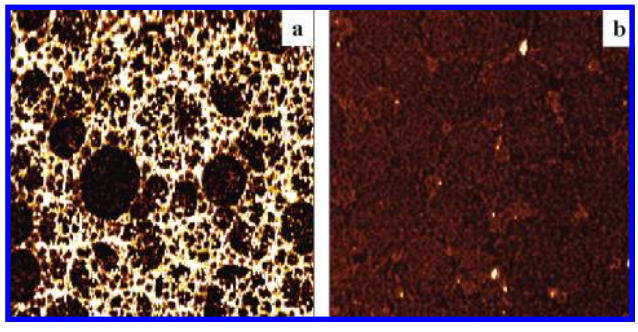

Figure 1. (a) AFM phase image of film−air interface of model PSA 2, and (b) film−air interface after soaking in solvent for 5 min. (Scan size 2.5 μm × 2.5 μm.)

Experimental Methods

Materials. Model water-based PSAs were synthesized at Franklin International (Columbus, OH) from the acrylic monomers *n*-butyl acrylate, vinyl acetate and methacrylic acid and a combination an anionic surfactant, disodium (nonylphenoxypolyethoxy)ethyl sulfosuccinate (Aerosol A-103, CAS No. 9040-38-4) obtained from CYTEC Industries, Inc. (West Paterson, NJ), and a nonionic surfactant, nonylphenol polyethoxylate (IGEPAL CO-520, CAS No. 68412-54-4), obtained from Rhodia, Inc. (Cranbury, NJ). Three model systems are reported on here. They are all synthesized using identical synthesis approaches and conditions. The first model PSA system contains 100 wt % (i.e., 100 % of the total surfactant mass in the PSA) anionic surfactant, second model PSA is produced with an emulsifier combination of 50 wt % anionic and 50 wt % nonionic, and the third model PSA contains 90 wt % nonionic and 10 wt % anionic. The solids content of produced latexes were 60−63 wt %. Properties were characterized using techniques described in previous publications.[27−29] Solid adhesive was coated onto silicone release liner and dried in oven at 82 °C for 10 min to produce 1 mil (25.4 μm) thick films. The total surfactant content in films assuming complete retention is 1.8 wt %. For analysis, films were transferred coated onto glass slides. These are identified throughout the paper as draw-down films. Several PSA film samples were prepared via spin coating on AFM specimen disks. These films are approximately 10 μm

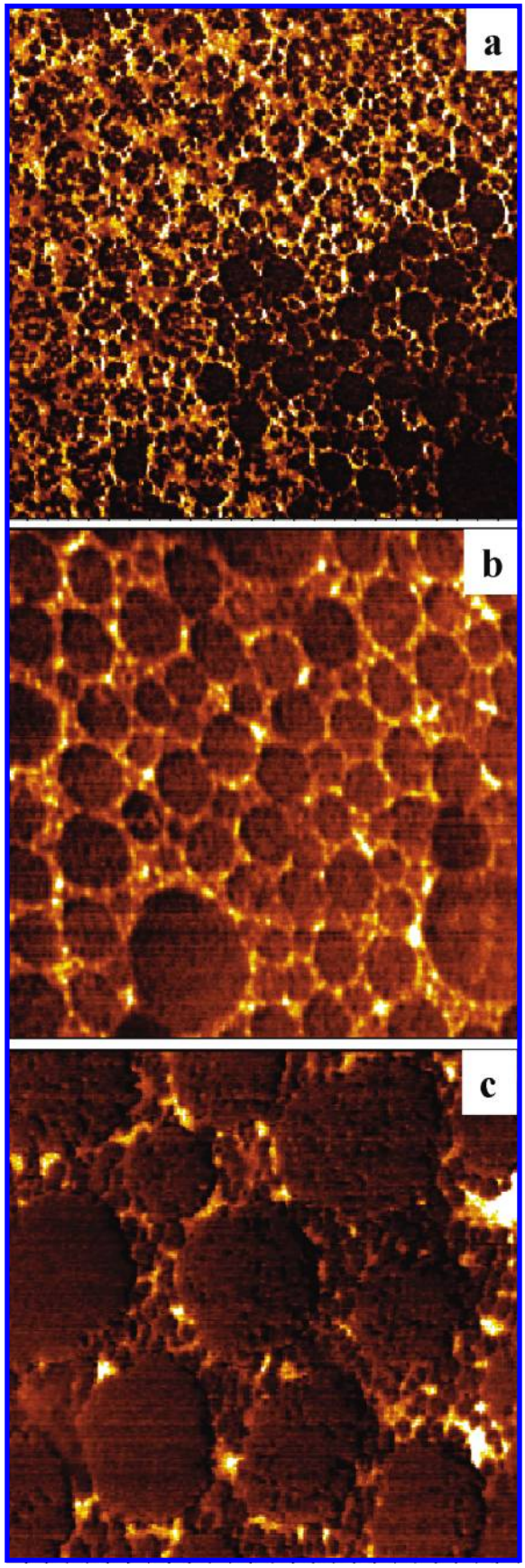

Figure 2. Atomic force microscopy phase images of film−air interfaces for drawdown coatings of (a) PSA 1, (b) PSA 2 and (c) PSA 3. (Scan size 2.5 μm × 2.5 μm.)

thick and were used for the initial surface morphology examination using AFM.

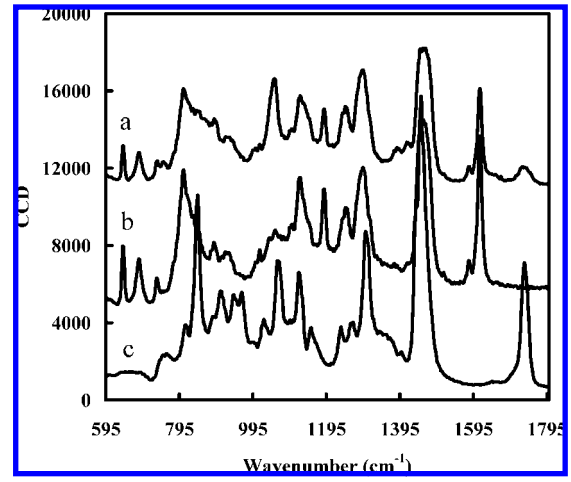

Figure 3. Basic Raman spectra of (a) anionic surfactant, (b) nonionic surfactant, and (c) soap-free latex.

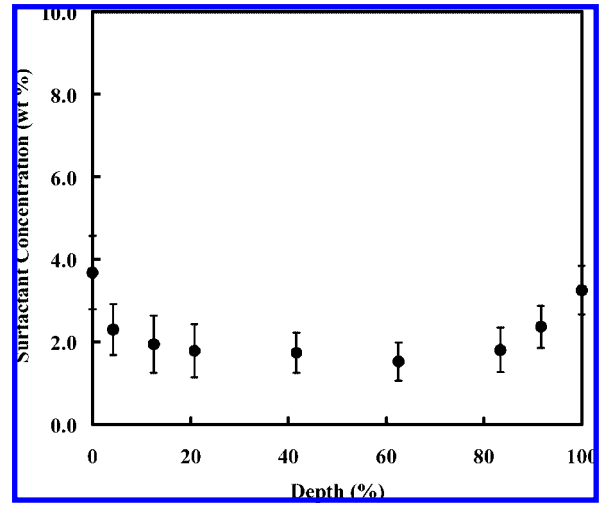

Figure 4. Surfactant distribution profile over the entire thickness of a film cast from PSA 1.

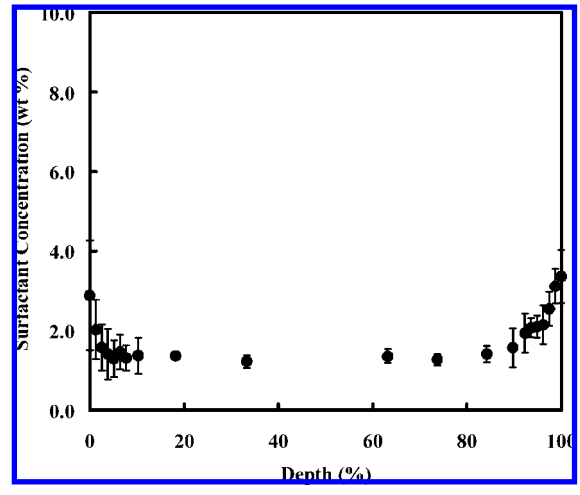

Figure 5. Surfactant distribution profile over the entire thickness of a film cast from PSA 2.

Determination of Surfactant Molar Mass and Relative Mobility. A liquid chromatography−mass spectroscopy (LC-MS) system was employed to check the molar mass distribution and formulas of anionic and nonionic surfactants used in PSA emulsions. A reverse phase high performance liquid chromatography (RP HPLC) method was used to separate samples of

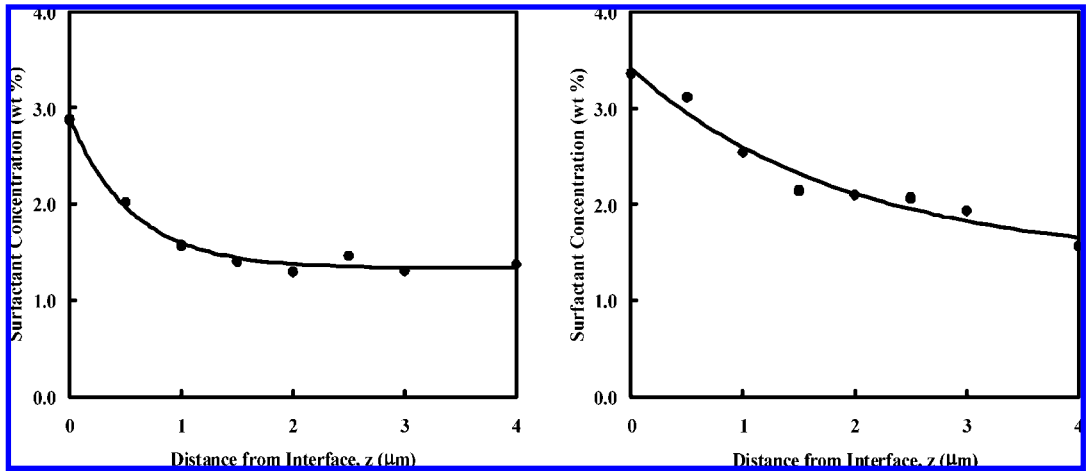

Figure 6. Fit of surfactant distribution for PSA 2 at (a) the film−air and (b) film−substrate interfaces using exponential decay model.

TABLE 3: Parameters from Fit with Exponential Decay Model

fitting parameters		PSA 1	PSA 2	PSA 3
film−air interface	C_0 (wt %)	1.84	1.34	1.41
	A (wt %)	1.84	1.56	0.88
	α (μm^{-1})	1.37	1.79	0.61
film−substrate interface	C_0 (wt %)	1.43	1.41	
	A (wt %)	1.83	2.00	
	α (μm^{-1})	0.36	0.52	

anionic and nonionic surfactants mixture using a SpectraSYSTEM P4000 LC (Thermo-Electron, Waltham, MA) to determine the retention time of surfactants. Before testing, pH values of anionic surfactant, nonionic surfactant and 50/50 anionic/nonionic surfactants mixture were adjusted to between 4 and 5, which is consistent with pH level of latex emulsion. A Zorbax Eclipse XD8-C8, 25 × 4.6 mm × 5 μm, column (Agilent, Fort Worth, TX) was used and the surfactants were eluted with a mobile phase of solvent A [90% water and 10% Acetonitrile (ACN)] and solvent B [100% ACN] at a flow rate of 1.0 mL/min. Surfactants were separated using a linear gradient from 100% solvent A to 90% solvent B over 19 min. Solvent B was held for 3 min at 90% before returning to initial conditions. The column was equilibrated for 5 min before subsequent injections. Surfactants were detected using a Thermo-Electron LCQ Classic ion trap mass spectrometer (Thermofisher, Waltham, MA). Spectra were collected in the positive ionization electrospray (ESI) mode.

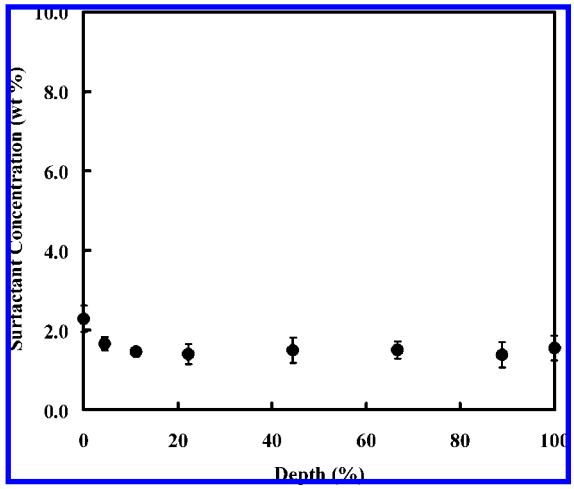

Figure 7. Surfactant distribution profile over the entire thickness of a film cast from PSA 3.

Atomic Force Microscopy Imaging of Film Surfaces. Atomic force microscopy was used to examine surface morphologies of PSA films. Using a PicoPlus PicoSPM (Agilent Technology, Foster City, CA) system, AFM imaging was performed in an environmental chamber with controlled temperature and relative humidity (RH). Intermittent contact or AC mode AFM was utilized. The amplitude of the cantilever is maintained constant during the scanning and the displacement of the piezo scanner through the feedback circuit to maintain this amplitude is recorded as a height image. The phase lag between the cantilever response and the driving oscillation signal is recorded as a phase image. Viscoelastic properties of the surface may also be evaluated from AFM phase images. All tapping mode AFM images presented in this paper were obtained employing integrated silicon cantilevers with tip radii of curvature 5−10 nm. The spring constant of the cantilever was manufacturer-specified in the range of 30−60 N/m and the measured resonant frequency was within 10% of 300 KHz. Here all PSA films were examined at ambient conditions.

Confocal Raman Microscopy Characterization of Surfactant Distributions. An alpha 300R confocal Raman microscope equipped with a UHTS200 spectrometer and a DV401 CCD detector from WITec (Ulm, Germany) was employed to collect single Raman spectra from the pure latex (synthesized by soap free emulsion polymerization method), pure surfactant (supplied by Franklin International), and the model PSA films. A Nikon 100x oil immersion objective was used for all measurements. An Ar-ion laser with the wavelength of 514.5 nm and maximum power of 50 mW was used for excitation. The lateral resolution of the confocal Raman microscope according to the theory of light diffraction is about 250 nm and the vertical resolution is about 500 nm. Since the sampling volume may be smaller than the average particle size of the latex spheres, measurements were conducted on several random locations on the film to minimize the variation. The Raman spectra of all samples, including the pure latex, pure surfactant and the film samples were recorded with an integration time of 240 s and laser power of 20 mW.

A set of latex films with defined concentration of surfactants ranging from 1 to 10% by weight was cast on glass slides. Pure latex with a solid content of 52 wt % was synthesized by soap free emulsion polymerization. A surfactant mixture containing 50 wt % anionic and 50 wt % nonionic surfactant was added in the pure latex at concentrations of 1%, 2%, 4%, 6%, and 10%. These were used to obtain a calibration curve for the calculation

of surfactant concentration in the dry PSA draw-down films. Curve fitting software is applied to calculate the ratio of the absorbencies of the surfactant to the polymer peaks. The ratio of the absorbencies of the surfactant to the polymer was then plotted as a function of the ratio of the concentrations and fit with a linear model. The ratio of molar absorption coefficients of surfactant to polymer was calculated from this curve as 0.5733, which is used for the calculation of the concentration of surfactant in the model PSA films from the confocal Raman spectra.

Results and Discussion

Properties of Emulsifiers and their Influence on PSA Films. Table 1 lists properties of surfactants used in the synthesis of the PSAs. Industrial surfactants are provided with a range of molar masses differing primarily by the number of ethoxylate linkages present. Both the number average (M_n) and weight average (M_w) molar masses obtained from LC-MS data are listed in Table 1. Nonionic surfactants tend to have lower critical micelle concentrations (CMCs) and hydrophilic−lipophilic balance (HLB) values than anionic surfactants possessing similar structures (i.e., similar hydrophobes). This reflects their generally greater hydrophobicity. From the table it can be seen that this general observation is consistent with the properties of the surfactant pair used here. Also listed in the table are estimated log K_{ow} values for both surfactants,[30] where K_{ow} is the octanol−water distribution coefficient. (log K_{ow} values have been shown to correlate with water solubility for organic liquids as well as their tendency to distribute into nonpolar phases.[31−34]) The value for the nonionic species is higher than that for the anionic surfactant consistent with its less polar structure. However the presence of a strong acidic functional group, which will be ionized over a wide pH range, substantially enhances the solubility of the anionic species and decreases its tendency to partition into a nonpolar phase. This is discussed further below.

The influence of the different surfactants on performance properties of PSA films cast is shown in Table 2. These properties for PSA 2, containing a 50:50 (wt %) mixture of the anionic and nonionic surfactant, and PSA 1, produced solely with anionic surfactant, are quite similar. While PSA 3, containing a blend of surfactants composed primarily of the nonionic surfactant, has a larger latex particle size. This PSA has a higher shear, a gauge of cohesive strength, which is likely a result of its high molar mass and/or gel content,[35,36] which are higher relative to those for PSAs 1 and 2. The differences in molar mass for PSA adhesive polymers may possibly impact surfactant distribution as was suggested by Tzitzinou et al.[37] However, by combining results for the adhesive films examined here, underlying trends are distinguishable. Also shown in Table 2 are contact angles for water on the 3 model PSAs. Increasing the concentration of surfactant will tend to raise the surface energy of a water-based, acrylic film likely due to an increasing concentration of the surfactant at the interface.[38] The interpretation of these values is complicated by the presence of the 2 different surfactants. However, it can be seen that the lowest angle is found for PSA1 and the highest for PSA 3 would appear to indicate higher concentrations of anionic surfactant result in a greater impact on the surface energy. Furthermore, when the films are rinsed with water, the angles are found to increase for all of the PSAs except that for PSA 3, which contains primarily nonionic surfactant, and the soap free PSA has a contact angle with water of about 112°, the same as that for PSA 3.

A "water-flux" mechanism has been proposed previously as a mechanism for the transport of surfactant from the aqueous phase to the film−air interface in PSA films.[39] As the film is dried water is drawn to the surface and evaporates leading to the precipitation of surfactant. Thus it would be expected that the surfactant species with the higher concentration in the aqueous phase will become enriched to a greater extent on the surface of the film.

In emulsion polymerization, emulsifiers (surfactants) are added above their CMC and form micelles, which house reacting monomer. Subsequent to polymerization, the emulsifiers stabilize the latex, and in addition to being physically sorbed at the particle−water interface, surfactant molecules may become more intimately tied into the polymer bead. The extent of this interaction determines the extent to which surfactant can be released into the aqueous phase as the interface is consumed by the coalescence process. It has been reported that nonionic surfactants tend to concentrate less than anionic surfactants at latex film surfaces. This has been attributed to inhibited migration for the nonionic species, consistent with a stronger interaction with the polymer phase.[40] Studies examining the sorption behavior of nonylphenol ethoxates at concentrations near and above their CMCs, indicate that species with lower ethoxylate contents have a higher affinity for substrates such as silicates, soils and sediments.[41−43] This is attributed to the increased hydrophobicity associated with these structural changes.

For this study, the anionic species contains a greater number of ethoxylate linkages as well as acid functional groups. It is well-known that for aqueous organic acids, the extent of sorption to natural substrates such as soils, sediments and wood correlates with measures of the acid's hydrophobicity, and it is commonly found that the conjugate base of the acid demonstrates little affinity for the same surfaces.[44,45] Results from RP HPLC carried out on an equal mass mixture of the 2 surfactants at the same pH as the PSA latexes demonstrate that the nonionic surfactant has a significantly greater affinity for the nonpolar stationary phase in that it elutes several column volumes subsequent to the anionic surfactant and only after significant modifications to the mobile phase. This is consistent with its higher log K_{ow} value and the fact that at least one of the anionic surfactant's acid functional groups is ionized greatly enhancing its tendency to partition into the aqueous phase. Thus, if the distribution of surfactant species in the films is strongly dependent on their relative affinity to the polymer phase, significant differences will be apparent in the films cast from the three latexes studied here. The anionic surfactant should deposit at the interfaces at substantially higher levels relative to the nonionic surfactant. Given the different concentrations of anionic and nonionic surfactant used, the model films should provide a decent gauge of the ability of AFM imaging and CRM depth profiling analysis to measure surfactant distribution behavior.

Imaging of Surfactant at Film Surfaces. In tapping mode AFM, the cantilever can be driven to interact with the surface in two distinct regimes, namely the attractive regime (or noncontact regime) in which the net interaction between AFM tip and the sample is attractive, and the repulsive regime (or intermittent-contact regime) in which a solid−solid mechanical contact is made and the net interaction is repulsive. When operating in repulsive regime, the viscous or more energy dissipative material often results in less phase lag, which produces a dark contrast on the phase image, while stiff or less energy dissipative materials provides bright contrast. When operating in attractive regime, the phase contrast is usually reversed. The tapping strength or the tip−sample interaction force varies with the free oscillation amplitude (A_0) of the

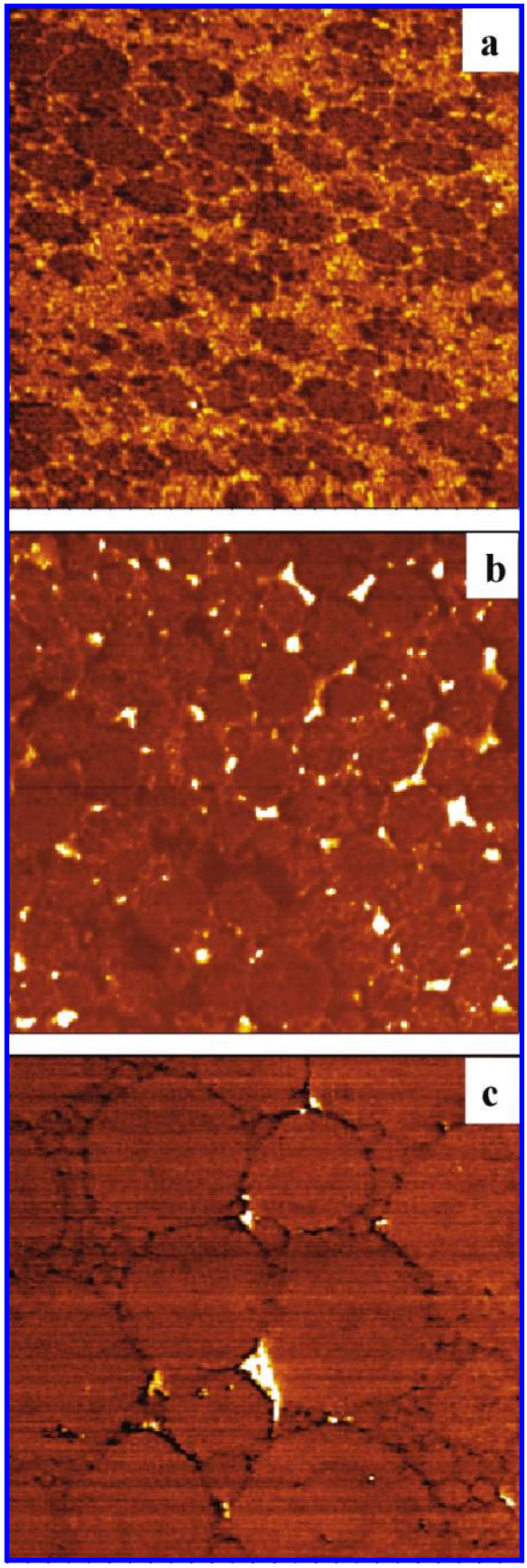

Figure 8. (a) AFM phase images of film−substrate interface of drawdown coatings of (a) PSA 1, (b) PSA 2, and (c) PSA 3. (Scan size 2.5 μm × 2.5 μm.)

cantilever and the amplitude ratio of set-point oscillation A and A_0. For the AFM phase images presented here, the cantilever was operated in the repulsive regime with free oscillation amplitude of 300 nm and $A/A_0 \sim 0.9-0.95$.

An AFM phase image of a spin coated, 50:50 wt % anionic: nonionic PSA film, PSA 2, obtained under ambient conditions (45% relative humidity) is shown in Figure 1a. The image was recorded at the film−air interface. Dark regions with spherical geometry can clearly be seen. These circular regions have diameters of 200−800 nm, which matches the particle size distribution obtained using dynamic light-scattering carried out on the latex emulsion (Table 2). Near spherical geometry and a well-spaced distribution indicate that the coalescence of latex beads has not occurred, nor has particle compaction. The second phase (bright contrast corresponding to less energy dissipative regions) appears to be the surfactant domain. The combination of an abundant presence of surfactants between and on the surface of latex beads and lack of particle coalescence indicates a likely connection. In order to verify this assumption, a small amount of ethyl alcohol (3 mL) was applied to the surface of the spin-coat model PSA 2 film for short time periods (5 min) and removed by further spin-coating. Here ethanol is used instead of water to rinse the top surface of PSA film because it more efficiently removed the surfactant. The phase image of the rinsed surface is shown in Figure 1b. With 5 min of solvent soaking and then rinsed by spin coating, the boundaries of latex particles are nearly absent, consistent with coalescence of the latex particles. These observations are a direct indication of the coalescence inhibition mechanism induced by the presence of surfactant. It is consistent with the conclusions from the study conducted by Mallégol et al. on the film formation and surface morphology of water-based PSA film.[16−18] It is interesting that the surfactant forms a compact, more elastic structure relative to the latex spheres. Varying tapping strength (A/A_0) during the imaging also showed significantly greater compressibility of particle domains.

Figure 2 shows AFM phase images of film−air interfaces of all model PSA draw-down films. It can be seen that the latex beads in nonionic dominant PSA film, PSA 3, are much larger than those that contain more anionic surfactant. As was expected, the amount of surfactant aggregated at this interface is significantly larger for PSA 1 (Figure 2a), followed by PSA 2 (Figure 2b), and little surfactant is apparent at the interface of PSA 3 (Figure 2c). This would indicate a greater tendency of the anionic surfactant to locate at the film surface, which is consistent with the contact angle data reviewed previously.

Characterizing Surfactant Distribution with Confocal Raman Microscopy. Figure 3 is a collection of basic Raman spectra for the pure latex and surfactants. The peaks at 1612 and 1735 cm^{-1} are assigned to an aromatic C−C, on-ring stretch mode for the surfactant and carbonyl stretch mode of the polymer, respectively. The ratio of the absorbencies of the 1612 and 1735 cm^{-1} peaks are used to quantify the surfactant concentration across the film thickness. It was found that the ratio of any two polymer peaks across the film remains constant. The concentration profile of surfactants in PSA 1 and PSA 2 drawn-down films are shown in Figures 4 and 5, respectively. It should be noted that the draw-down PSA films are analyzed from the film−air interface, i.e., 0% corresponds to the film−air interface and 100% to the film−substrate interface. At least five locations were randomly selected on each film and Raman measurements were done with 0.5−5 μm increments across the film thickness. The data shown in the figures are the average values obtained from at least five Raman measurements and the error bar is estimated variation of the data. All of the profiles show an enrichment of the surfactant at the interfaces and even

distribution in the bulk film. However, the data variation at the interfaces is much higher than that in the bulk film. The concentrations of surfactants drop significantly over a short distance from film−air interface and level at about the 10−20% thickness point. A similar profile is found, but the shape of the concentration curve is distinctly different, rising more gradually at the film−substrate interface. In these two PSA films, surfactant enrichment is almost on the same level at film−air and film−substrate interfaces. However, it is evident that surfactant aggregation at the interfaces of PSA 1 is higher than that of PSA 2. This is consistent with the AFM observations, in which the aggregation of the surfactant at the film−air interface of PSA 1 was more significant than that of PSA 2 (Figure 2, parts a and b). Similar findings were also reported by Tzitzinou and Blaroui,[46,47] who studied the fate of anionic surfactants during film formation of acrylic latexes.

In order to better understand surfactant migration mechanism, more detailed analyses were carried out at the surfactant enrichment layers for both interfaces. It is found that the surfactant distribution curves are well fit by an exponential decay model shown in Figure 6 for model PSA 2. At both interfaces, the surfactant distribution follows an exponential decay model, i.e.,

$$C(z) = C_0 + A \exp(-\alpha z) \quad (1)$$

where $C(z)$ is surfactant concentration at a depth z from the interface, C_0 is the bulk phase surfactant concentration, and A and α are fitting constants indicating the maximum enrichment of surfactant and rate of decay, respectively. For the film−air interface of PSA 2, $C_0 = 1.34$ wt %, $A = 1.56$ wt %, and $\alpha = 1.79\ \mu m^{-1}$, while for the film−substrate interface of PSA 2, $C_0 = 1.41$ wt %, $A = 2.00$ wt %, and $\alpha = 0.52\ \mu m^{-1}$. The fitting parameters for model PSA 1 and 3 were also listed in Table 3. (For all 3 PSAs, r^2 values for the model fits were >0.97.) The differences in the shape of the surfactant distributions between the film−air and film−substrate are more quantitatively demonstrated by the model.

Films cast with PSA 3 where the nonionic surfactant dominates the binary mixture, only a small surfactant enrichment is found at the film−air interface, as shown in Figure 7. The surfactant is distributed nearly evenly over the bulk film. These results are consistent with those reported by Evanson et al.,[24] who systematically investigated mobility of anionic and nonionic surfactants in ethyl acrylate/methyl acrylic acid latex films using FTIR-ATR. Since they did not have information about the depth profile, they concluded nonionic surfactant distributed evenly in the bulk film because surfactant enrichment was not found at film−air and film−substrate interfaces. A study on emulsion polymerization of styrene and methacrylic acid carried out with polyoxyethylene nonyl phenyl ether nonionic emulsifier found that nonionic surfactant is incorporated inside latex particles.[40] The amount of nonionic emulsifier that partitioned into the latex particles reached as high as 75 wt % of total surfactant utilized. The lower HLB number of the nonionic surfactant, the greater the amount incorporated inside latex particles,[48] and it is difficult for these species to elute unless facilitated by higher temperatures. The smaller standard deviation of the data shown in the Figure 7 is consistent with a more even lateral distribution of the nonionic surfactant, which would be achieved by its incorporation into latex beads. It can be concluded that the small surfactant enrichment at the film−air interface observed for PSA 3 is likely caused by the 10 wt % anionic surfactant in the blend. AFM observation is consistent with this assessment and strongly supports the results from Raman depth profiling of PSA films (Figure 2c and Figure 8c).

The results presented above indicate that nonylphenol ethoxylate surfactants tend to concentrate at film interfaces. The Raman depth profiling of surfactants also demonstrates that surfactant enrichment at the interfaces of PSA film depends primarily on the relative percent of anionic surfactant in the total surfactant content; the more anionic surfactant in the blend, the more significant the surfactant segregation. This is consistent with the water-flux mechanism. As mention above, anionic surfactant is more water soluble and hydrophilic especially given the ionization of at least one of its acid functional groups, and thus these molecules are more apt to be found in the aqueous phase available to be carried to the film−air interfaces during water evaporation. However, it still remains to be determined whether the surfactant fate is a matter of kinetics with drying conditions and film structure pushing the distribution toward a metastable state. The films analyzed with CRM were all cast on release liner possessing a surface energy of about 20 mJ/m^2. It is interesting that the anionic surfactant migrates to both interfaces to almost the same extent. Figure 8 shows the AFM imaging of film−substrate interfaces of all model PSA drawdown films. The images are consistent with CRM depth profiling of surfactants in the model PSA films with PSA 1 demonstrating that highest surfactant content at the film−substrate interface followed by PSA 2. Little surfactant is found at the film−substrate interface for PSA 3.

Acknowledgment. We thank Dr. Thomas Krick, Biochemistry Department, University of Minnesota, for running and interpreting the LC-MSdata and Dr. Yanhong Gu, Beijing Institute of Petrochemical & Technology, for help in processing Raman data. This research was financially supported in part by the U.S. Department of Energy, Project Number DE-FC36-04GO14309.

References and Notes

(1) Staicu, T.; Micutz, M.; Leca, M. *Prog. Org. Coat.* **2005**, *53*, 56–62.
(2) Charmeau, J. Y.; Berthet, R.; Gringreau, C.; Holl, Y.; Kientz, E. *Int. J. Adhes. Adhes.* **1997**, *17*, 169–176.
(3) Tobing, S. D.; Klein, A. *J. Appl. Polym. Sci.* **2001**, *79*, 2230–2244.
(4) Mulvihill, J.; Toussaint, A.; Wilde, M. D. *Prog. Org. Coat.* **1997**, *30*, 127–139.
(5) Donkus, L. J. *Adhes. Age* **1997**, *32*, 35–37.
(6) Kientz, D.; Holl, Y. *Colloids Surf. A* **1993**, *78*, 255–270.
(7) Holl, Y. *Macromol. Symp.* **2000**, *151*, 473–478.
(8) Guigner, D.; Fischer, C.; Holl, Y. *Langmuir* **2001**, *17*, 6419–6425.
(9) Wheeler, O. L.; Jaffe, H. L.; Wellman, N. *Off. Dig.* **1954**, *26*, 1239–1241.
(10) Voyutskii, S. S. *J. Polym. Sci.* **1958**, *32*, 528–534.
(11) Keddie, J. L. *Mater. Sci. Eng.* **1997**, *3*, 101–170.
(12) Zhao, C. L.; Dobler, F.; Pith, T.; Holl, Y.; Lambla, M. *J. Colloid Interface Sci.* **1989**, *128*, 437–449.
(13) Kunkel, J. P.; Urban, M. W. *J. Appl. Polym. Sci.* **1993**, *50*, 1217–1223.
(14) Belaroui, F.; Cabane, B.; Dorget, M.; Grohens, Y.; Marie, P.; Holl, Y. *J. Colloid Interface Sci.* **2003**, *262*, 409–417.
(15) Belaroui, F.; Hirn, M. P.; Grohens, Y.; Marie, P.; Holl, Y. *J. Colloid Interface Sci.* **2003**, *261*, 336–348.
(16) Mallégol, J.; Gorce, J.-P.; Dupont, O.; Jeynes, C.; McDonald, P. J.; Keddie, J. L *Langmuir* **2002**, *18*, 4478–4487.
(17) Mallégol, J.; Dupont, O.; Keddie, J. L. *Proceedings of the 28th Coating Science and Technology*; Athens, Greece, 2002.
(18) Mallégol, J.; Dupont, O.; Keddie, J. L. *J. Adhesion Sci. Technol.* **2003**, *17*, 243–259.
(19) Urban, M. W. *Prog. Org. Coat.* **1997**, *32*, 215–229.
(20) Zhao, C. L.; Holl, Y.; Pith, T.; Lambla, M. *Colloid Polym. Sci.* **1987**, *265*, 823–829.
(21) Tebelius, L. K.; Urban, M. W. *J. Appl. Polym. Sci.* **1995**, *56*, 387–395.
(22) Amalvy, J. I.; Soria, D. B. *Prog. Org. Coat.* **1996**, *28*, 279–283.
(23) Evanson, K. W.; Thorstenson, T. A.; Urban, M. W. *J. Appl. Polym. Sci.* **1991**, *42*, 2297–2307.
(24) Lee, W. P.; Gundabala, V. R.; Akpa, B. S.; Johns, M. L.; Jeynes, C.; Routh, A. F. *Langmuir* **2006**, *22*, 5314–5320.

(25) Belaroui, F.; Grohens, Y.; Boyer, H.; Holl, Y. *Polymer* **2000**, *41*, 7641–7645.

(26) Schmidt, U.; Hild, S.; Ibach, W.; Hollricher, O. *Macromol. Symp.* **2005**, *230*, 133–143.

(27) Guo, J.; Severtson, S. J.; Gwin, L. E. *Ind. Eng. Chem. Res.* **2007**, *46*, 2753–2759.

(28) Guo, J.; Severtson, S. J.; Kroll, M. S. *Ind. Eng. Chem. Res.* **2004**, *43*, 1443–1450.

(29) Nowak, M. J.; Severtson, S. J.; Wang, S. P.; Kroll, M. S. *Ind. Eng. Chem. Res.* **2003**, *42*, 1681–1687.

(30) Schwarzenbach, R. P.; Gschwend, P. M.; Imboden, D. M. *Environmental organic chemistry*, John Wiley & Sons, Inc.: New York, 1992.

(31) Leo, A.; Hansch, C.; Elkins, D. *Chem. Rev.* **1971**, *71*, 525–616.

(32) Valkó, K. *J. Chromatogr. A* **2004**, *1037* (1−2), 299–310.

(33) Ahel, M.; Giger, W. *Chemosphere* **1993**, *8*, 1471–1478.

(34) Ruiz-Angel, M. J.; Carda-Broch, S.; Garcia-Alvarez-Coque, M. C.; Berthod, A. *J. Chromatogr. A* **2005**, *1063*, 25–34.

(35) Shen, H.; Zhang, J.; Liu, S.; Liu, G.; Zhang, L. *J. Appl. Polym. Sci.* **2008**, *107*, 1793–1802.

(36) Gonzalez, I.; Leiza, J. R.; Asua, J. M. *Macromolecules* **2006**, *39*, 5015–5020.

(37) Tzitzinou, A.; Keddie, J. L.; Geurts, J. L.; Mulder, M.; Satguru, R.; Treacher, K. E. *Film Formation in Coatings*; ACS Symposium Series 790; American Chemical Society: Washington, DC, 2001.

(38) Guo, J.; Severtson, S. J.; Gwin, L. E.; Houtman, C. J. *Ind. Eng. Chem. Res.* **2008**, *47*, 2612–2617.

(39) Kientz, E.; Holl, Y. *Colloids Surf. A: Physicochem. Eng. Aspects* **1993**, *78*, 255–270.

(40) Okubo, M.; Furukawa, Y.; Shiba, K.; Matoba, T. *Colloid Polym. Sci.* **2003**, *281*, 182–186.

(41) Kibbey, T. C. G.; Hayes, K. F. *J. Contam. Hydrol.* **2000**, *41*, 1–22.

(42) Kibbey, T. C. G.; Hayes, K. F. *J. Colloid Interface Sci.* **1998**, *197*, 210–220.

(43) Kibbey, T. C. G.; Hayes, K. F. *J. Colloid Interface Sci.* **1998**, *197*, 198–209.

(44) Severtson, S. J.; Banerjee, S. *Environ. Sci. Technol.* **1996**, *30*, 1961–1969.

(45) Westall, J. C.; Leuenberger, C. J.; Schwarzenbach, R. P. *Environ. Sci. Technol.* **1985**, *19*, 193–198.

(46) Tzitzinou, A.; Jenneson, P. M.; Clough, A. S.; Keddie, J. L.; Lu, J. R.; Zhdan, P.; Treacher, K. E.; Satguru, R. *Prog. Org. Coat.* **1999**, *35*, 89–99.

(47) Belaroui, F.; Grohens, Y.; Marie, P.; Holl, Y. *Prog. Colloid Polym. Sci.* **2004**, *128*, 159–162.

(48) Okubo, M.; Chaiyasat, A.; Yamada, M.; Suzuki, T.; Kobayashi, H. *Collid Polym. Sci.* **2007**, *285*, 1755–1761.

JP804876X